Corrosion Science xxx (2010) xxx–xxx

Contents lists available at ScienceDirect

Corrosion Science

journal homepage: www.elsevier.com/locate/corsci

Classification of corrosion defects in NiAl bronze through image analysis

Ramana M. Pidaparti [a,*], Babak Seyed Aghazadeh [a], Angela Whitfield [b], A.S. Rao [b,1], Gerald P. Mercier [b]

[a] Department of Mechanical Engineering, Virginia Commonwealth University, 401 West Main Street, Richmond, VA 23284, USA
[b] Department of Alloy Development and Mechanics, Carderock Division, Naval Surface Warfare Center, 9500 Mac Arthur Blvd, West Bethesda, MD 20817, USA

ARTICLE INFO

Article history:
Received 22 March 2010
Accepted 7 July 2010
Available online xxxx

Keywords:
A. Nickel
B. SEM
B. Modeling Studies
C. Pitting Corrosion
C. Acid Corrosion
C. Corrosion Fatigue

ABSTRACT

Corrosion surface damage in the form of pitting and micro-cracks is observed in many metals. Cracks usually initiate from the pits and grow under cyclic stresses and eventually lead to material failure. An image analysis based on wavelet transforms and fractals was used to study the corrosion morphology of nickel aluminum bronze metal under varying corrosion conditions and applied stresses. Image feature parameters were extracted and analyzed to classify the pits/cracks in the metal samples. The results obtained indicate that classification of pits/cracks is possible with image analysis and may be used for correlating service/failure conditions based on corrosion morphology.

1. Introduction

Engineering components made from nickel aluminum bronze (NAB) metal are being used in the Navy's ship and propeller components due to their high toughness. However, this metal is subjected to pits and stress corrosion cracking due to the operating conditions of salt water environment. In order to reduce the maintenance requirements, expedite repair, and extend the life of naval nickel aluminum bronze components, engineering studies are being carried out to investigate the mechanism of stress corrosion crack initiation through experiments and modeling.

Pitting and stress corrosion cracking are known to be some of the major damage mechanisms affecting the integrity of NAB materials and structures in nuclear and naval engineering. Corrosion pits generally initiate due to some chemical or physical heterogeneity at the surface, such as inclusions, second phase particles, flaws, mechanical damage, or dislocations. Many NAB alloys contain numerous constituent particles, which play an important role in corrosion pit formation [1–5]. To better understand particle-induced pitting corrosion, optical microscopy, Scanning Electron Microscopy (SEM) and Transmission Electron Microscopy (TEM) techniques have been used. Due to operating and special service environments (e.g. saltwater), corrosion pits and stress corrosion cracking are readily formed between the constituent particles and the surrounding matrix in these alloys [5].

Micro-cracks usually initiate from the corrosion pit sites in the material. Under the interaction of cyclic load and the corrosive environment, cyclic loading facilitates the pitting process, and corrosion pits, acting as geometrical discontinuities, lead to crack initiation and propagation and then final failure [6–9]. Corrosion can lead to accelerated failure of structural components under fatigue loading conditions. Understanding and predicting corrosion damage morphology in the form of pits/cracks is therefore very important for the structural integrity of materials and structures. Electrochemical probe techniques such as Scanning Reference Electrode Technique (SRET), Scanning Vibrating Electrode Technique (SVET), and Localized Impedance Spectroscopy (LEIS) [10–13] have been used for electrochemical measurements at the metal surface. There are no probe related techniques that quantitatively assess the corrosion morphology in the form of pits and stress corrosion cracking in metals. Recently, Pidaparti et al. [14,15] developed a computational methodology to predict stresses around pits and found that pit induced stresses reaches a plateau after certain corrosion time and may lead to crack initiation after that, and this phenomena changes with corrosion environment.

Image analysis has been used to characterize corrosion morphology in materials subjected to a variety of environmental conditions. Kapsalas et al. [16] proposed a method to detect corrosion size and topology in stonework surfaces by testing and evaluating image segmentation schemes. They have showed that their results are in good agreement with assessments based on chemical analyses performed on the same surfaces. Choi et al. [17] have analyzed the corrosion surface damage using digital image processing techniques. They employed HIS model interpretation, co-occurrence matrix, and multidimensional scaling proce-

* Corresponding author. Tel.: +1 804 827 3742; fax: +1 804 827 7030.
E-mail address: rmpidaparti@vcu.edu (R.M. Pidaparti).
[1] Present address: Nuclear Regulatory Commission, Washington, DC, USA.

0010-938X/$ - see front matter © 2010 Elsevier Ltd. All rights reserved.
doi:10.1016/j.corsci.2010.07.017

Report Documentation Page

Form Approved
OMB No. 0704-0188

1. REPORT DATE	2. REPORT TYPE	3. DATES COVERED
MAR 2010		**00-00-2010 to 00-00-2010**

4. TITLE AND SUBTITLE	5a. CONTRACT NUMBER
Classification of corrosion defects in NiAl bronze through image analysis	5b. GRANT NUMBER
	5c. PROGRAM ELEMENT NUMBER
6. AUTHOR(S)	5d. PROJECT NUMBER
	5e. TASK NUMBER
	5f. WORK UNIT NUMBER

7. PERFORMING ORGANIZATION NAME(S) AND ADDRESS(ES)	8. PERFORMING ORGANIZATION REPORT NUMBER
Naval Surface Warfare Center Carderock Division,Department of Alloy Development and Mechanics,9500 Mac Arthur Blvd,West Bethesda,MD,20817	
9. SPONSORING/MONITORING AGENCY NAME(S) AND ADDRESS(ES)	10. SPONSOR/MONITOR'S ACRONYM(S)
	11. SPONSOR/MONITOR'S REPORT NUMBER(S)

12. DISTRIBUTION/AVAILABILITY STATEMENT

Approved for public release; distribution unlimited

13. SUPPLEMENTARY NOTES

14. ABSTRACT

Corrosion surface damage in the form of pitting and micro-cracks is observed in many metals. Cracks usually initiate from the pits and grow under cyclic stresses and eventually lead to material failure. An image analysis based on wavelet transforms and fractals was used to study the corrosion morphology of nickel aluminum bronze metal under varying corrosion conditions and applied stresses. Image feature parameters were extracted and analyzed to classify the pits/cracks in the metal samples. The results obtained indicate that classification of pits/cracks is possible with image analysis and may be used for correlating service/failure conditions based on corrosion morphology.

15. SUBJECT TERMS

16. SECURITY CLASSIFICATION OF:			17. LIMITATION OF ABSTRACT	18. NUMBER OF PAGES	19a. NAME OF RESPONSIBLE PERSON
a. REPORT	b. ABSTRACT	c. THIS PAGE			
unclassified	**unclassified**	**unclassified**	**Same as Report (SAR)**	**6**	

dure to characterize images by three categories of colour, texture, and shape features. Wang et al. [18] used wavelet packet decomposition energies of images at different wavelet sub-bands as features to study the atmospheric corrosion behavior of zinc samples. They acquired a relationship between the selected image features and the corrosion weight loss. Tao et al. [19] analyzed the atmospheric corrosion of field exposure high strength aluminum alloys. They used wavelet packed decomposition energies at different sub-bands to estimate the corrosion loss of five types of aluminum alloys. It was found that the values of sub-image energies decreased with increasing exposure time. There are no studies in the literature on classification of pits/cracks in NAB metals under combined corrosion and cyclic stresses.

In order to qualitatively and quantitatively characterize the early stage damage mechanisms in NAB metals under corrosion and cyclic stresses, image analysis of corrosion morphology may be used as a tool to predict the nucleation of cracks resulting from initiation and growth of pits. In this study, image analysis based on wavelet transforms and fractals was used to study the corrosion morphology of Nickel Aluminum Bronze metal under varying corrosion conditions and applied cyclic stresses. Image feature parameters were extracted and analyzed to classify the pits/cracks in the NAB metal samples.

2. Image analysis methods

Several image analysis methods are available for characterizing the corrosion surface morphology. In this study, wavelet transforms and fractals were used for the image analysis based on our experience, and are described below briefly.

2.1. Wavelet packet transform

In order to improve the images obtained from microscopy techniques such as SEM and others, multi-resolution wavelet transforms can be used. The details of standard wavelet transformations can be found in the literature [20]. As an extension of the standard wavelets, wavelet packets (WPs) which represent a generalization of the multi-resolution analysis use the entire family of sub-band decompositions to generate a complete representation of images. There are many outstanding properties of wavelet packets, which encourage researchers to employ them in widespread fields. It has been shown that sparsity of coefficients' matrix, computational efficiency, multiresolution and time–frequency analysis can be useful in dealing with many engineering problems. The hierarchical WP transform uses a family of wavelet functions and their associated scaling functions to decompose the original time series/signal into subsequent sub-bands. The decomposition process is recursively applied to both the low and high frequency sub-bands to generate the next level of the hierarchy.

Two-dimensional discrete wavelet packet transform (DWPT) decomposition allows us to analyze an image simultaneously at different resolution levels and orientations. In 2-D DWPT method, an image is decomposed into one approximation and three detail images. The approximation and the detail images are then decomposed into a second-level approximation and detail images, and the process is repeated. The standard 2-D DWPT can be implemented with a low-pass filter and a high-pass filter [20]. The 2-D DWPT of an $N \times M$ discrete image A up to level $P+1$ ($P \leqslant \min(\log_2 N, \log_2 M)$) is recursively defined in terms of the coefficients at level p as follows:

$$C^{p+1}_{4k,(i,j)} = \sum_m \sum_n h(m)h(n)C^p_{k,(m+2i,n+2j)}$$
$$C^{p+1}_{4k+1,(i,j)} = \sum_m \sum_n h(m)g(n)C^p_{k,(m+2i,n+2j)}$$
$$C^{p+1}_{4k+2,(i,j)} = \sum_m \sum_n g(m)h(n)C^p_{k,(m+2i,n+2j)}$$
$$C^{p+1}_{4k+3,(i,j)} = \sum_m \sum_n g(m)g(n)C^p_{k,(m+2i,n+2j)} \quad (1)$$

where C^0_0 is the image A and k is an index of the nodes in the wavelet packet tree denoting each sub-band. h and g are the filter coefficients of low-pass and high-pass filters, respectively. Supposing that Haar basis has been used, $h = \{-0.7071, 0.7071\}$, and $g = \{0.7071, 0.7071\}$. At each step, the image C^p_k is decomposed into four quarter-size images C^{p+1}_{4k}, C^{p+1}_{4k+1}, C^{p+1}_{4k+2}, and C^{p+1}_{4k+3}. The capital letters (N or M) are maximum constants defined by the image size. However, small letters (m or n) are defined at each step. For example, when $p = 5$, p can be 1, 2, 3, or 4 and so on.

The Shannon entropy in different sub-bands is computed from the sub-band coefficient matrix as:

$$Entropy_p(k) = -\sum_i \sum_j |C^p_{k,(i,j)}|^2 \log |C^p_{k,(i,j)}|^2 \quad (2)$$

$$Energy_p(k) = \sum_i \sum_j |C^p_{k,(i,j)}|^2 \quad (3)$$

where $Energy_p(k)$ and $Entropy_p(k)$ are the energy and entropy of the image projected onto the subspace at node (p,k). The entropy of each sub-band provides a measure of the image characteristics in that sub-band. The energy distribution has important discriminatory properties for images and as such can be used as a feature for texture classification. From the equations above, it follows that the wavelet entropy is minimum when the image represents an ordered activity characterized by a narrow frequency distribution, whereas the entropy is high when an image contains a broad spectrum of frequency distribution.

In this study, firstly the SEM images of the surfaces have been transformed from TIF to JPG to export to MATLAB software. Haar mother wavelet was employed to decompose the grayscale corrosion images to the second level of decomposition and Shannon entropies of sub-images at each sub-band have been used as image features. The process has been done using the wavelet toolbox of MATLAB software on a Pentium Dual-Core and 1.66 GHz processor speed PC computer.

2.2. Fractal analysis

The fractal dimension (FD) is a mathematical concept to classify certain sets in more detail than the topological dimension can. There are many interesting and aesthetic examples of such sets (known as "fractal sets") that can be created. Many scientists in life and material sciences and engineering use the fractal dimension (FD) as a parameter to characterize rough lines or surfaces. In other words, the fractal dimension is a measure of the morphology, texture, and roughness in the surface (or images). FD can numerically characterize the variation in surface structure caused by corrosion, which corresponds to morphology changes in grey value images captured by microscopy techniques such as SEM or AFM. Various methods have been proposed to estimate fractal values [21]: Fourier, Kolmogorov, Korcak, Minkowski, root mean square, slit island, etc. These methods differ in computational efficiency, numerical precision and estimation boundary. However, a strong correlation was reported between the relative ranking of fractal values obtained from different fractal measuring techniques [21,22]. Among these methods the Fourier analytical technique is the most promising one in that it has several advantages. First, the Fourier method is relatively insensitive to the presence of noise in images; second, there exists a fast algorithm, the FFT, which provides efficient implementation particularly for online application; and third, the computation of fractal values is based on an explicit formula

Please cite this article in press as: R.M. Pidaparti et al., Classification of corrosion defects in NiAl bronze through image analysis, Corros. Sci. (2010), doi:10.1016/j.corsci.2010.07.017

and is potentially more accurate computationally. For these reasons Fourier analysis was adopted to estimate fractal values in this study.

For a surface image $f(x,y)$, the power spectral density (PSD) is calculated as:

$$S(u,v) = |F(u,v)|^2, \quad (4)$$

where $F(u, v)$ is the Fourier transform of $f(x, y)$, and u and v are the spatial frequencies (number of waves per unit wave length) in the x and y directions, respectively. The PSD $S(u, v)$ is converted to the polar coordinate system $S(f)$ such that $f = \sqrt{u^2 + v^2}$. The values of $S(f)$, at each radial frequency f, are averaged over angular distributions. For a fractal surface, the power spectrum shows a linear variation between the logarithm of $S(f)$ and the logarithm of the frequency f [23]. The slope of the linear regression line β is related to the FD by equation [24]:

$$FD = (7 - \beta)/2 \quad (5)$$

In this study, FD analysis was carried out on SEM images of corroded specimens under varying conditions with a goal of differentiating pits and cracks in them.

3. Experimental data

Nickel aluminum bronze alloy metal samples were cut into 50 mm × 5 mm × 1 mm dimensions from a plate. The chemical composition of the NAB plate (wt.%) [1] is 8.7–9.5% Al; 4.0–4.8% Ni; 3.5–4.3% Fe; 1.2–2.0% Mn; 0.1% Si; 0.02% Pb and the rest is Cu with an average tensile strength of 731 MPa and Rockwell B Hardness of 203 (HRB). The NAB plate's typical microstructure consists of continuous equiaxed crystals with small areas of metastable b phases. k Phase precipitates are found at grain boundaries in a phase and b phases areas [1]. Initially, the specimens were first inspected visually and diamond polished up to a surface finish of 3 μm before the corrosion testing. These specimens were immersed in 10% ammonia (NH_4OH) (by vol.) – 90% seawater (by vol.) prepared as per ASTM D1141 standard and the cyclic stress was applied under three point bending according to ASTM G39. The chemical composition of the simulated seawater is as follows: initially salt solution was prepared using salts NaCl 0.413 mol dm^{-3}; $MgCl_2$ 0.0546 mol dm^{-3}; Na_2SO_4 0.0288 mol dm^{-3}; $CaCl_2$ 0.0105 mol dm^{-3}; and KCl 0.0009 mol dm^{-3}, and dissolving them in 1000 mL of de-ionized distilled water. Concentrated ammonia solution of 100 mL was then added to 900 mL of the salt solution to obtain the simulated.

After exposing the specimens for a specific corrosion time (1–37 days) under specified cyclic stress (0–310 MPa), the samples were examined under SEM to characterize the surface morphology. The experiments were conducted by the researchers at the Department of Alloy Development and Mechanics, Carderock Division, Naval Surface Warfare Center, Bethesda, Maryland. They provided the SEM image data to VCU for further analysis. An investigation of the SEM data for defects classification was carried out in this study. The corrosion morphology of typical NAB specimens with defects, pits, and cracks is shown in Fig. 1. These SEM images were used in the image analysis to develop features to characterize the pits/cracks in NAB metal.

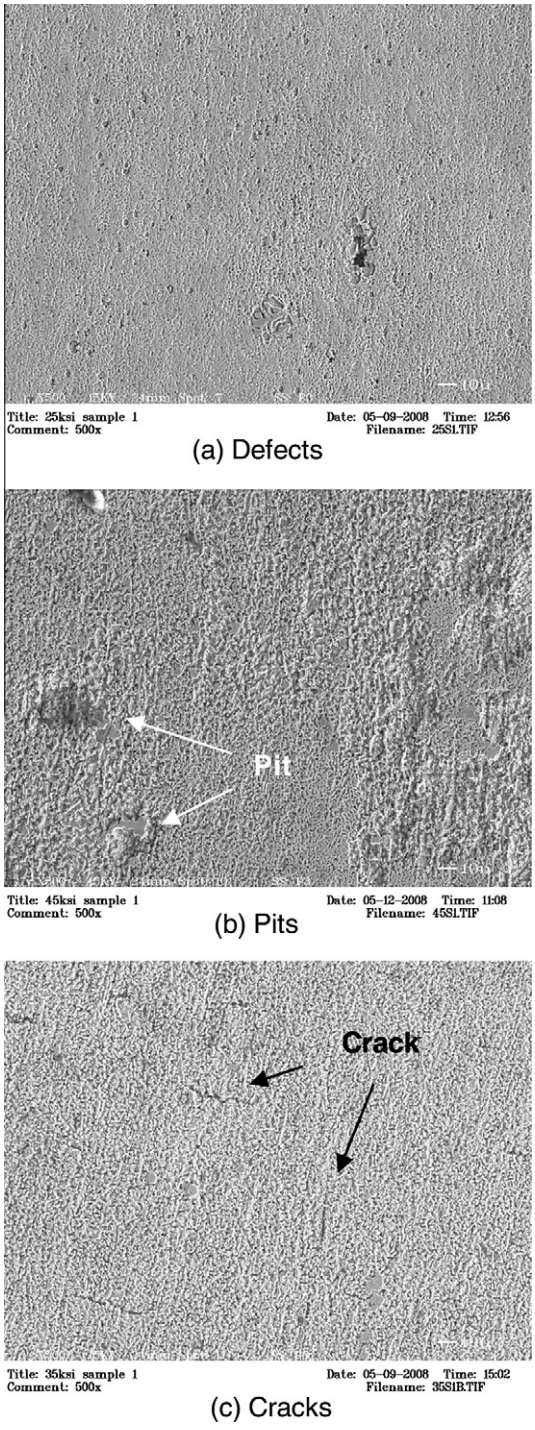

Fig. 1. Surface morphology of corroded NAB specimens.

4. Results and discussion

4.1. Defect detection

In order to study the effect of cyclic stress on the corrosion rate of samples, the images of samples were decomposed using 2D wavelet packet decomposition. Shannon entropies of sub-images were then calculated at each sub-band. Fractal dimensions of the images as well as the Shannon entropies of wavelet packet decompositions of images were used as potential features. Fig. 2 shows the Shannon entropies of four sub-images of wavelet packet decomposition plotted against cyclic stress for samples after one time step. It can be seen from Fig. 2 that the metal samples under the stresses of 170, 240, and 310 MPa have higher entropies in comparison with other samples and are most likely candidates to have defects. Therefore, by observing the SEM images corresponding to these stresses, defects, pits, and cracks can be recognized as shown in Fig. 1. Interestingly, these findings of no cracks, and

Please cite this article in press as: R.M. Pidaparti et al., Classification of corrosion defects in NiAl bronze through image analysis, Corros. Sci. (2010), doi:10.1016/j.corsci.2010.07.017

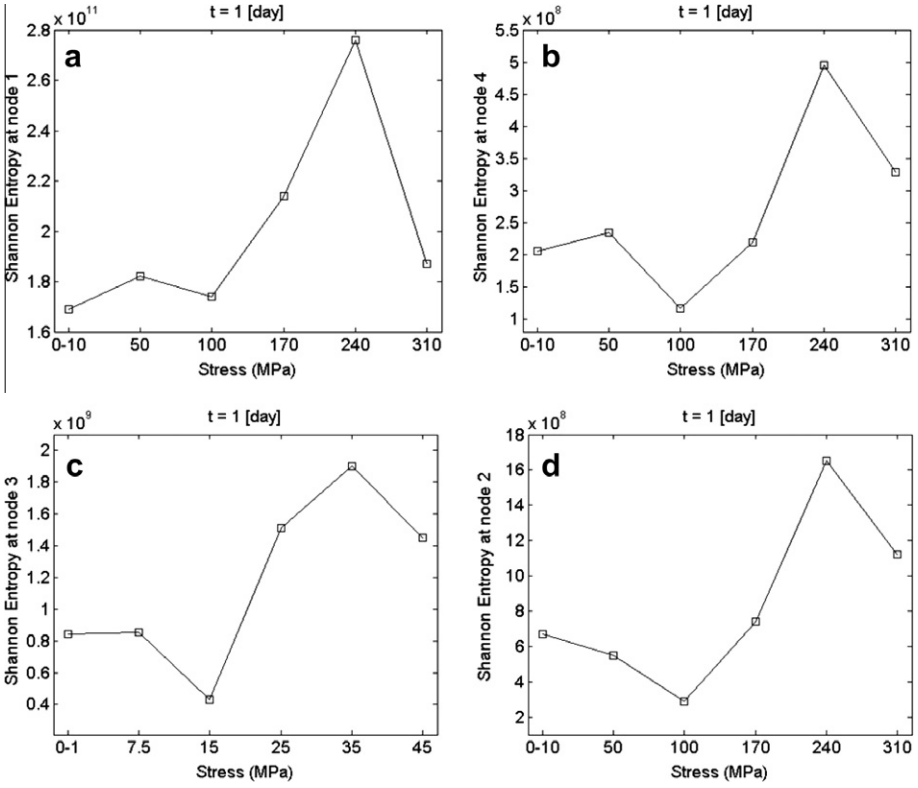

Fig. 2. Shannon entropies of four sub-images calculated from wavelet image analysis with varying applied cyclic stresses of NAB specimens.

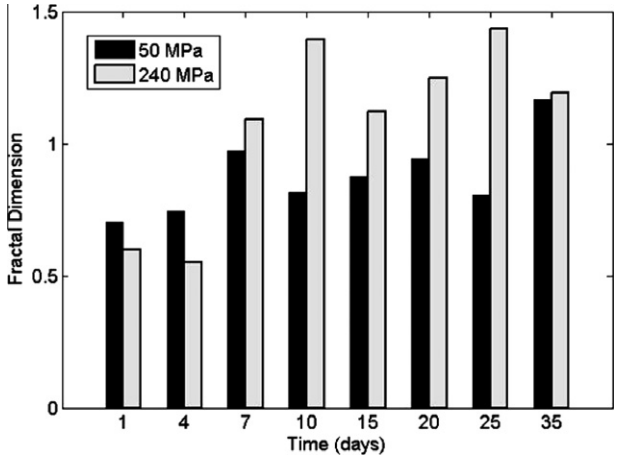

Fig. 3. Fractal dimension calculated from fractal analysis with varying corrosion time (time step – number of corrosion days) under applied cyclic stresses.

cracks has been observed by Vasanth and Hays [1] in their studies on NAB metal under varying environmental conditions.

Cyclic stress levels of 50, and 240 MPa were chosen to show the effect of corrosion time on surface morphology of the NAB metal samples. Fractal Dimensions of images were calculated using Eq. (5) and plotted against corrosion time in Fig. 3. It can be seen from Fig. 3 that the fractal dimensions of corroded images of NAB metal specimens have a roughly increasing trend with time. Also, when SEM images with high fractal dimensions were observed, defects in the samples were clearly visible, whereas SEM images with low fractal dimensions did not show any visible damage on the surfaces of metal samples.

4.2. Crack/pit classification

The classification of cracks/pits was investigated through image analysis of corroded specimen SEM images. The procedure used to establish the defect classification (pits versus cracks) is shown in Fig. 4. Twelve sub-images, six containing cracks, and six containing pits, were analyzed. Each image's size was 256 × 256 pixels. Fig. 5 shows the typical images containing normal, pits, crack-pit, and cracks extracted from the entire corroded specimen under varying time and cyclic stresses. Fractal dimensions on these images were calculated and presented in Fig. 6. It can be seen from Fig. 6 (a) that fractal dimension increases for cracks and pits in comparison to

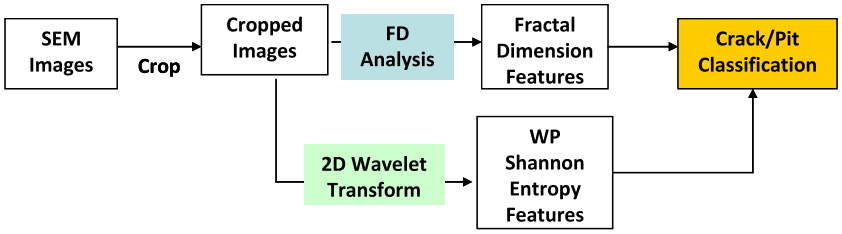

Fig. 4. Overview of the defect classification procedure for NAB specimens.

Please cite this article in press as: R.M. Pidaparti et al., Classification of corrosion defects in NiAl bronze through image analysis, Corros. Sci. (2010), doi:10.1016/j.corsci.2010.07.017

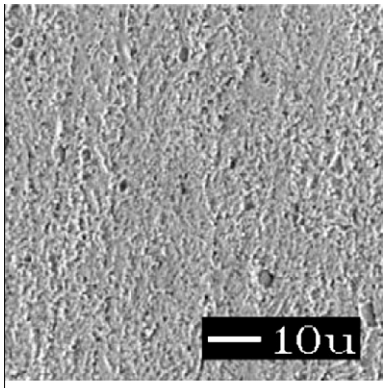

Normal

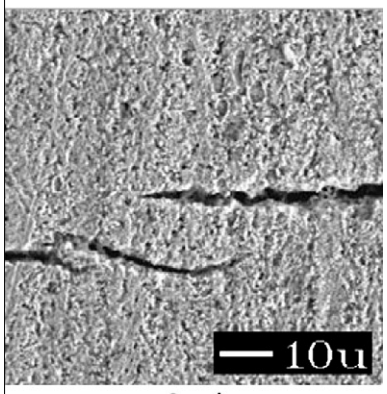

Crack

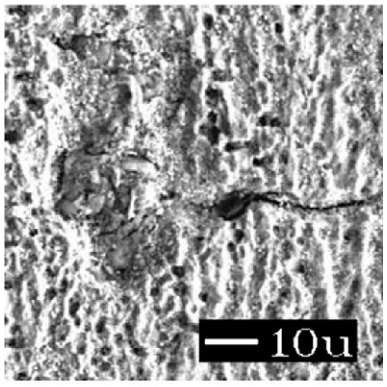

Crack-Pit

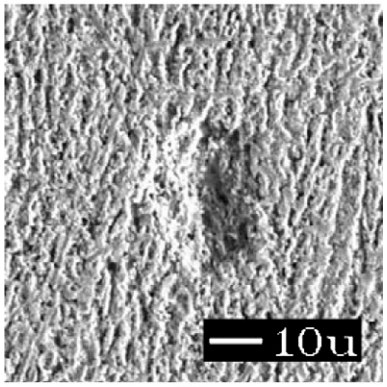

Pit

Fig. 5. Typical defects (normal (no defect), pits, cracks-pits, and cracks) observed in NAB metal specimens under combined corrosion and cyclic stresses.

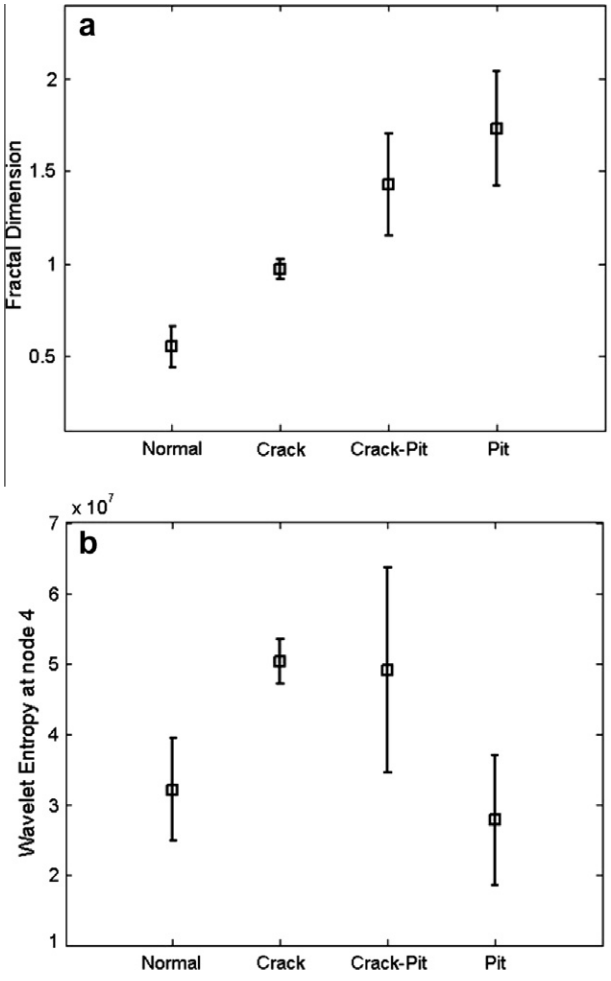

Fig. 6. (a) Fractal dimension and (b) Shannon entropy calculated from the images of Fig. 5 classifying various defects.

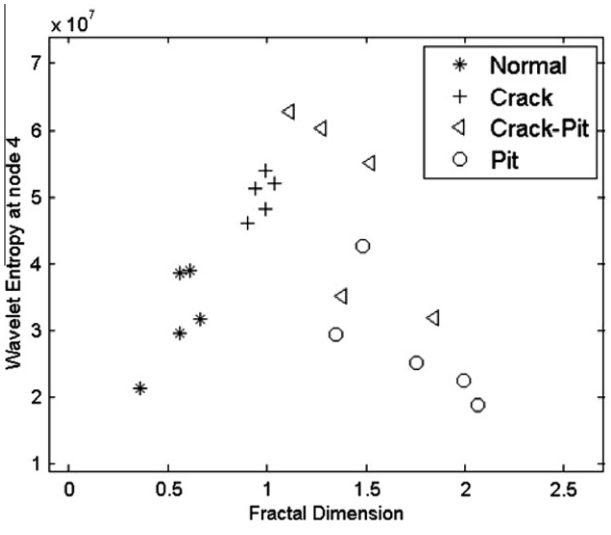

Fig. 7. Two-dimensional projection of image features (fractal dimension and Shannon entropy) for classifying pits/cracks in NAB metal samples.

Please cite this article in press as: R.M. Pidaparti et al., Classification of corrosion defects in NiAl bronze through image analysis, Corros. Sci. (2010), doi:10.1016/j.corsci.2010.07.017

normal (no defect) images. Also, the images with pits have higher fractal dimensions in comparison to images with cracks. The samples are linearly separable in this feature space and a threshold can be chosen to distinguish cracks from pits and its transition. This shows the effectiveness of the fractal dimension feature in the classification of corrosion cracks from pits and their transition.

In addition to fractal dimension, the Shannon entropies of the wavelet packet decompositions of images containing normal (no defects), pits, cracks, and combination of pit-crack cases (Fig. 5) were also calculated. It can be seen from Fig. 6(b) that the cracks have higher entropies in comparison to pits in comparison to normal (no defect) in their images. It has been observed that with only increasing corrosion, there are visible pits in SEM images. In contrast, when the cyclic stress is increased, there are visible cracks and pits in SEM images. To provide a better illustration, a two dimensional projection of images (normal (no defects), pits, cracks, and combination of pit-crack cases) into the feature space is presented in Fig. 7 for the images considered in this study. It can be seen from Fig. 7 that using the features of fractal dimension and Shannon entropy of the wavelet packet decomposition, cracks and pits are linearly separable and, thus, easily classifiable.

5. Conclusions

An image analysis based on wavelet transforms and fractals was used to study the corrosion morphology of nickel aluminum bronze metal under varying corrosion conditions and applied cyclic stresses. Image feature parameters were extracted from the experimental data obtained from SEM, and analyzed to classify the pits/cracks in the metal samples. The results obtained from image analysis indicate that classification of pits/cracks is possible as they are linearly separable based on the fractal dimension and entropy features. The approach presented in this paper may be used for correlating service/failure conditions based on corrosion morphology in metals. However, more research is needed to study further the proposed methods/analysis based on images obtained from non-destructive inspection devices as part of routine inspection and correlating the fractal dimension to service/failure conditions.

Acknowledgements

The first two authors thank US National Science Foundation for supporting this work through a Grant DMR-0505496. The authors also acknowledge the financial support from Dr. Airan Perez, Program Officer, Office of Naval Research, Virginia.

References

[1] K.L. Vasanth, R.A. Hays, Corrosion assessment of nickel–aluminum bronze (NAB) in Seawater, Corrosion 2004, Paper No. 04294.
[2] F.M. Dersch, A. Cohn, Ultrasonic Inspection of Nickel Aluminum Bronze for Stress Corrosion Cracking, NSWCCD-61-TR-2001-21, 2001.
[3] M.D. Fuller, S. Swaminathan, A.P. Zhilyaev, T.R. McNelley, Microstructural transformations and mechanical properties of cast nial bronze: effects of fusion welding and friction stir processing, Mater. Sci. Eng. 463 (1-2) (2007) 128–137.
[4] J.A. Wharton, R.C. Barik, G. Kear, R.J.K. Wood, K.R. Stokes, F.C. Walsh, The corrosion of nickel–aluminum bronze in seawater, Corros. Sci. 47 (2005) 3336–3367.
[5] K. Oh-Ishi, T.R.T.R. McNelley, Microstructural modification of as-cast NiAl bronze by friction stir processing, Metall. Mater. Trans. 35 (2004) 2951–2961.
[6] G.T. Burstein, C. Liu, R.M. Souto, S.P. Vines, Origins of pitting corrosion, Corros. Eng. Sci. Technol. 39 (2004) 25.
[7] S.I. Rokhlin, J.Y. Kim, H. Nagy, B. Zoofan, Effect of pitting corrosion on fatigue crack initiation and fatigue life, Eng. Fract. Mech. 2 (1999) 425–444.
[8] S. Ishihara, S. Saka, Z.Y. Nan, T. Goshima, S. Sunada, Prediction of corrosion fatigue lives of aluminum alloy on the basis of corrosion pit growth law, Fatigue Fract. Eng. Mater Struct. 29 (2006) 472–480.
[9] M.R. Sriraman and R.M. Pidaparti, Life prediction of aircraft aluminum subjected to pitting corrosion under fatigue conditions, J. Aircraft (7–8) (2009) 1253–1259.
[10] H.S. Isaacs, Initiation of stress corrosion cracking of sensitized type 304 stainless steel in ductile thiosulfate solution, J. Electrochem. Soc. 135 (1988) 2180–2183.
[11] T. Suter, H. Bohni, A new microelectrochemical method to study pit initiation on stainless steels, Electrochim. Acta 42 (1997) 3275–3280.
[12] R. Oltra, V. Vignal, Recent advances in local probe techniques in corrosion research – analysis of the role of stress on pitting sensitivity, Corros. Sci. 49 (2007) 158–165.
[13] C.H. Paik, R.C. Alkire, Role of sulfide inclusions on localized corrosion of Ni200 in NaCl solutions, J. Electrochem. Soc. 148 (2001) 276–281.
[14] R.M. Pidaparti, R.R. Patel, Correlation between corrosion pits and stresses in Al alloys, J. Mater. Lett. 62 (2008) 4497–4499.
[15] R.M. Pidaparti, K. Koombua, A.S. Rao, Corrosion pit induced stresses prediction from SEM and finite element analysis, Int. J. Comput. Methods Eng. Sci. Mech. 10 (2009) 117–123.
[16] K.Y. Choi, S.S. Kim, Morphological analysis and classification of types of surface corrosion damage by digital image processing, Corros. Sci. 47 (2005) 1–15.
[17] P. Kapsalas, M. Zervakis, P. Maravelaki-Kalaitzaki, Evaluation of image segmentation approaches for non-destructive detection and quantification of corrosion damage on stonework, Corros. Sci. 49 (2007) 4415–4442.
[18] S. Wang, S. Song, Image analysis of atmospheric corrosion exposure of zinc, Mater. Sci. Eng. A 385 (2004) 377–381.
[19] L. Tao, S. Song, X. Zhang, Z. Zhang, F. Lu, Image analysis of atmospheric corrosion of field exposure high strength aluminum alloys, Appl. Surf. Sci. 254 (2008) 6870–6874.
[20] S. Mallat, A Wavelet Tour of Signal Processing, Academic, New York, 1999.
[21] J. Zhang, P. Regtian, M. Korsten, Monitoring of dry sliding wear using fractal analysis, in: 10th TC-10 IMEKO Conference on Technical Diagnostics, 9–10 June 2005, Budapest, Hungary.
[22] J. Rawers, J. Tylczak, Fractal characterization of wear-erosion surfaces, Mater. Eng Performance 8 (6) (1999) 669–676.
[23] J.C. Russ. Fractal Surfaces. Plenum Press, New York, 1994.
[24] H. Peitgen, D. Saupe, M.F. Barnsley, The Science of Fractal Images, Springer-Verlag, New York, 1988.

Please cite this article in press as: R.M. Pidaparti et al., Classification of corrosion defects in NiAl bronze through image analysis, Corros. Sci. (2010), doi:10.1016/j.corsci.2010.07.017